Acoustic impedance measurements—correction for probe geometry mismatch

N. H. Fletcher,[a] J. Smith, A. Z. Tarnopolsky, and J. Wolfe
School of Physics, University of New South Wales, Sydney 2052, Australia

The effect of evanescent mode generation, due to geometrical mismatch, in acoustic impedance measurements is investigated. The particular geometry considered is that of a impedance probe with an annular flow port and a central microphone, but the techniques are applicable to other geometries. It is found that the imaginary part of the measured impedance error is proportional to frequency, and that the sign of the error is positive for measurements made on tubes with diameter much larger than that of the inlet port, but negative for tubes with diameter close to that of the inlet. The result is a distortion of the measured frequencies of the impedance minima of the duct while the maxima are largely unaffected. There is, in addition, a real resistive component to the error that varies approximately as the square root of the frequency. Experiment confirms the results of the analysis and calculations, and a calibration procedure is proposed that allows impedance probes that have been calibrated on a semi-infinite tube of one diameter to be employed for measurements on components with an inlet duct of some very different diameter. © *2005 Acoustical Society of America.* [DOI: 10.1121/1.1879192]

I. INTRODUCTION

The measurement of acoustic impedance is of great importance in many branches of the subject, typical cases being the input impedance of mufflers or, in contrast, of musical wind instruments. Most methods involve injecting a known acoustic flow and measuring the resultant acoustic pressure, the only significantly different approach being that using two spaced microphones in a tube leading to the device to be measured so as to evaluate the reflection coefficient. A treatment from the viewpoint of general acoustics has been given by Beranek,[1] and surveys from the more precise viewpoint of musical instrument acoustics by Benade and Ibisi[2] and by Fletcher and Rossing.[3] The resulting analysis is straightforward and the results reliable if the diameter of the impedance head duct through which the flow is injected is equal to the diameter of the inlet to the device under measurement, but such a match is not generally possible. In the case of a significant mismatch of diameters, or in geometry, there is a corresponding error in the measured acoustic impedance. It is the purpose of this note to calculate the effect of this geometrical mismatch and to show how the error can be compensated for by a simple calculation.

In the impedance-measuring heads with which one usually deals, as shown in Fig. 1, the acoustic flow is injected through a high acoustic resistance located coaxially with the pipe inlet to the object being measured, and with either a circular or annular cross-section, the latter having advantages because a very narrow annulus can be less than one viscous diffusion length in width, thus providing a high and nearly frequency-independent acoustic resistance.[4] A small microphone measures the pressure, either at the center of the face

of this inlet resistance or sometimes in an asymmetrical manner by being inserted from one side of the duct. The residual area of the pipe inlet is sealed by a flat rigid plate. For simplicity this situation will be idealized in what follows to planar probe geometry and the symmetrical microphone position shown in Fig. 1(a), though it is clearly possible to use the same techniques to calculate more complex geometries. Some such extensions are discussed.

II. EVANESCENT MODES

When a sound wave enters a pipe from a pipe of smaller diameter, localized modes are generated close to the inlet wall in the larger pipe. The effect in the smaller duct can be neglected here, since the injected acoustic flow is assumed to be constant across its whole area in impedance measuring devices. This situation is described by the wave equation in cylindrical polar coordinates,

$$\frac{1}{r}\frac{\partial}{\partial r}\left(r\frac{\partial p}{\partial r}\right) + \frac{1}{r^2}\frac{\partial^2 p}{\partial \phi^2} + \frac{\partial^2 p}{\partial x^2} = \frac{1}{c^2}\frac{\partial^2 p}{\partial t^2}, \tag{1}$$

where p is the acoustic pressure, c is the speed of sound in air, x is the axial coordinate, and r, ϕ are polar coordinates in the cross section. Since it has been assumed that there is no angular variation around the pipe, the coordinate ϕ can be neglected, and the solution has the form

$$p(x,r,t) = \sum_{n=0}^{\infty} A_n J_0(\alpha_n r/R)\exp[j(-k_n x + \omega t)] + B\exp[j(k_0 x + \omega t)], \tag{2}$$

where J_0 is the Bessel function of order zero, ω is the angular frequency of the signal, and A_n, α_n, and k_n are constants to be determined. The A_n are complex amplitudes associated with the injected wave, and the final term with complex am-
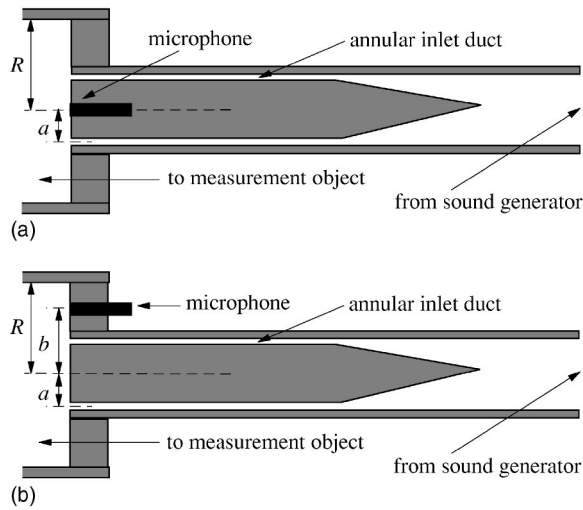
FIG. 1. (a) Geometry of a typical impedance probe connected to a duct of radius R. For the calculation the diameter $2a$ of the annulus that acts as the flow injection port is taken as 7 mm and the microphone diameter as zero. (b) An alternative geometry with the microphone displaced a distance b from the axis of the inlet annulus.

plitude B represents the reflected wave, assumed to be planar, which carries information about the acoustic impedance being measured. Restriction of the frequency range so that higher modes with $n>0$ are all nonpropagating and the returning wave is planar is necessary for the definition of acoustic impedance, since otherwise it would be a multiple-valued function with a different value for each propagating mode.

The values of the quantities α_n are derived from the assumed condition that the walls of the duct are rigid so that, taking the pipe radius to be R, it is required that $\partial p/\partial r=0$ at $r=R$ for each of the modes n. This leads to the condition

$$\left.\frac{dJ_0(\alpha_n r/R)}{dr}\right|_{r=R}=-\frac{\alpha_n}{R}J_1(\alpha_n)=0, \qquad (3)$$

and hence[5] to the series of approximate values 3.83, 7.02, 10.17,... for α_n. Substituting (2) back in (1) then leads to the result

$$k_n^2=\left(\frac{\omega}{c}\right)^2-\frac{\alpha_n^2}{R^2}. \qquad (4)$$

If the frequency is low enough that $\omega/c<\alpha_n/R$, then k_n becomes imaginary and the corresponding mode is nonpropagating or "evanescent." Such modes are exponentially attenuated along the axis of the pipe and are essentially confined to within an axial distance less than a few times R/α_n, or at most about one pipe-radius from the place where they are generated. In contrast, the plane-wave mode $n=0$, for which $\alpha_0=0$, propagates at all frequencies, although in this case k_0 is still complex because of wall losses along the tube and has the value[4,6]

$$k_0=\omega/c-j\frac{10^{-5}\beta\omega^{1/2}}{R}, \qquad (5)$$

where $\beta>1$ is a factor to allow for the nonideal smoothness of the walls. Typically $\beta\approx3$ for moderately smooth tubes.

In acoustic impedance measurements of the type with which we are concerned here, a one-dimensional plane-wave approximation is assumed in the object being studied, so attention is directed towards the plane wave amplitudes A_0 and B, with the other terms regarded as undesired byproducts of the mismatch between the impedance head and the entry duct. The aim of the present analysis is to identify the contributions of these higher modes and show how they can be corrected for.

To simplify matters, the inlet to the object under test is assumed to be an unobstructed circular tube of radius R with rigid boundaries, at least for a distance away from the measuring plane about equal to its radius. The impedance probe is also assumed to have circular symmetry, and a longitudinal cross section is shown in Fig. 1(a). The flow injection port is assumed to be a narrow annulus of radius a, and the radius of the central microphone diaphragm, assumed to be of very high acoustic impedance, is assumed to be sufficiently small that it can be taken as zero. Geometrical mismatch is then defined in terms of the ratio R/a.

The additional condition imposed by the rigid boundaries at the entry to the pipe is then that

$$\frac{\partial p}{\partial x}=0 \quad \text{if } x=0 \quad \text{and } r\neq a, \qquad (6)$$

while the boundary condition across the acoustic flow inlet at $x=0$ requires that

$$v(r)=\frac{U}{2\pi r}\delta(r-a) \qquad (7)$$

where U is the total acoustic inlet flow and $\delta(r-a)$ is the Dirac delta function. Now $\partial p/\partial x=-j\omega\rho v$, so that

$$\left.\frac{\partial p}{\partial x}\right|_{x=0}=-j\frac{\omega\rho U}{2\pi a}\delta(r-a). \qquad (8)$$

Combining (8) with (2), multiplying by $rJ_0(\alpha_n r/R)$, and integrating from 0 to R then gives

$$k_n A_n M_n-k_0 B M_0\delta_{n,0}=\frac{\omega\rho U}{2\pi}J_0\left(\frac{\alpha_n a}{R}\right), \qquad (9)$$

where,[7] since $J_1(\alpha_n)=0$ for all n,

$$M_n=\int_0^R J_0^2\left(\frac{\alpha_n r}{R}\right)r\,dr=\frac{R^2}{2}J_0^2(\alpha_n), \qquad (10)$$

and δ_{mn} is the Kronecker delta function which equals 1 if $m=n$ and 0 otherwise. Equation (9) then gives, for the case $n\neq0$,

$$A_n=\frac{\omega\rho U}{2\pi k_n M_n}J_0\left(\frac{\alpha_n a}{R}\right) \qquad (11)$$

and for the case $n=0$.

$$B=A_0-\frac{\omega\rho U}{2\pi k_0 M_0}. \qquad (12)$$

Now the measured value of the input impedance is

$$Z_{\text{meas}} = \left. \frac{p}{U} \right|_{x=0,r=0} = \frac{1}{U} \left(\sum_{n=0}^{\infty} A_n + B \right), \qquad (13)$$

while the true plane-wave impedance is

$$Z_{\text{true}} = \frac{A_0 + B}{U}. \qquad (14)$$

These equations can be combined to give

$$Z_{\text{meas}} = Z_{\text{true}} + \sum_{n=1}^{\infty} \frac{\omega \rho}{2 \pi k_n M_n} J_0 \left(\frac{\alpha_n a}{R} \right), \qquad (15)$$

and this equation will be the basis of the calculations to follow. A rather similar equation could be derived, following the same method, for other probe geometries, as discussed later. Despite the exponential decay of evanescent waves along the measurement axis, it is found by numerical exploration that a large number of modes must be taken into account to ensure smooth convergence. For the calculations to be reported later, 100 modes were included since the computation is quite simple.[8] A reasonable result can, however, be achieved with as few as ten modes.

This analysis is inapplicable at frequencies that are high enough that $k \geq \alpha_1 / R$, for then the evanescent modes begin to propagate and higher modes appear in the reflected wave. In practical terms, this occurs in a cylindrical conduit of radius R for frequencies above about $210/R$ Hz, where R is in meters. The analysis also omits consideration of viscous and thermal losses from the evanescent waves at the plane wall terminating the duct at $x=0$. A discussion of this point and an estimate of the form and magnitude of the resistive error is given in Sec. V. While, if the end wall is smooth and rigid, the resistive error contributed by these losses is very small compared with the imaginary part, its inclusion is found in Sec. VII to be necessary to give a complete measurement correction.

It is instructive to write the result (15) in terms of dimensionless parameters. Since the quantities α_n are dimensionless, it follows from (4) that we can write $k_n = R^{-1} f(\omega R/c)$, where the function f can be written down explicitly, while from (10), $M_n \propto R^2$. Thus (15) can be expressed in the form

$$Z_{\text{meas}} = Z_{\text{true}} + \frac{j \rho \omega}{a} G \left(\frac{R}{a}, \frac{\omega a}{c} \right), \qquad (16)$$

where the function $G(x,y)$ can be written explicitly. As will be shown below by means of a numerical calculation, the error term $Z_{\text{error}} = Z_{\text{meas}} - Z_{\text{true}}$ in (16) turns out to be almost exactly proportional to frequency over quite a large range of the ratio R/a, which implies that

$$\frac{Z_{\text{error}}}{Z_0(R)} \approx \frac{j \omega a}{c} F \left(\frac{R}{a} \right), \qquad (17)$$

where $Z_0(R) = \rho c / \pi R^2$ is the characteristic impedance of the pipe being measured, and the function $F(R/a)$ can be derived from Eqs. (15) and (16) and can be evaluated numerically. The form of this measurement error and its numerical evaluation will be discussed further in Sec. III.
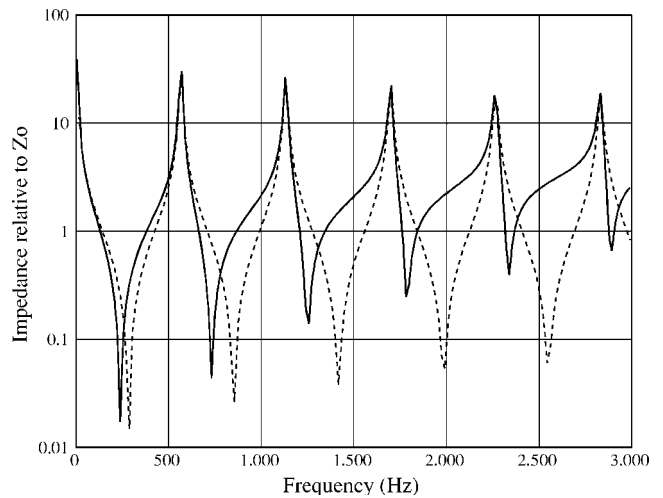

FIG. 2. Calculated magnitude of the impedance for a closed tube of diameter 50 mm and length 300 mm, as would be measured with an annular probe of diameter 7 mm. The broken curve shows the true impedance, assuming a wall loss factor of 3, while the full curve shows the impedance that would be measured.

III. A SPECIFIC EXAMPLE

It is interesting to examine the trend of the calculated results for cases in which the exact solution is known, and an obvious candidate is the simple stopped tube of length L and radius $R > a$, for which the input impedance is known to be

$$Z = -j \frac{\rho c}{\pi R^2} \cot(kL), \qquad (18)$$

where wall losses are taken into account as in Eq. (5).

For the specific case calculated, the tube to be measured was assumed to have a diameter of 53 mm and a length of 300 mm, while the input annulus was taken to have a diameter of 7 mm, this being a very substantial mismatch. The wall loss magnification factor β of (5) in the tube being measured is taken to have the value $\beta = 3$, which is fairly typical for tubes of the particular material used. The calculated results for the magnitude of the measured impedance and that of the actual plane-wave impedance are shown in Fig. 2. As will be discussed later, it is necessary to include almost 100 terms in the summation in (15) in order to achieve an accurate result, but this presents no computational difficulty, and indeed a summation with only ten terms gives moderate accuracy. The impedance can readily be split into real and imaginary parts in the calculation if desired. The first higher mode becomes propagating at about 8 kHz in the case of this tube, so the measurement is necessarily limited to significantly below this frequency. Clearly there is a very large discrepancy between the true and measured impedance values even below 3 kHz, so that the measurement in its unadjusted state is of little use unless one is interested simply in the frequencies of the impedance maxima.

Let the acoustic impedance of the device being measured be $Z_{\text{sub}} = R_{\text{sub}} + j X_{\text{sub}}$, with appropriate descriptive subscripts. Then exploration of the reactive part of the measurement error $X_{\text{error}} = X_{\text{meas}} - X_{\text{true}}$ as a function of frequency and of the tube diameter mismatch shows that the error is quite closely proportional to frequency over the frequency
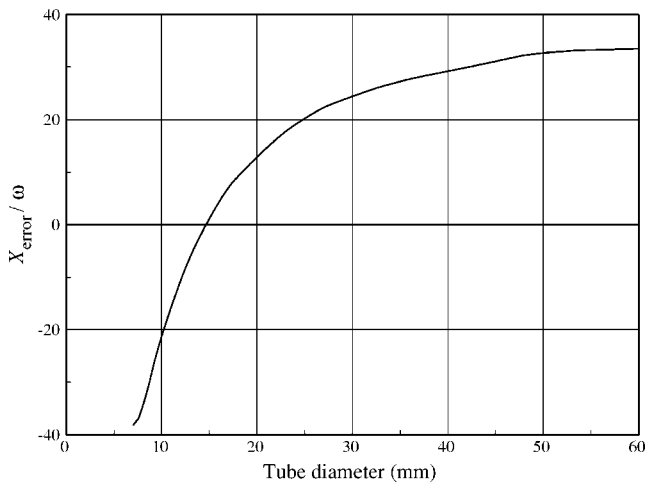
J. Acoust. Soc. Am., Vol. 117, No. 5, May 2005

Fletcher *et al.*: Acoustic impedance measurements   2891

FIG. 3. Calculated frequency-weighted error X_{error}/ω in the imaginary part of the impedance (in units of $\text{Pa s}^2 \text{m}^{-3}$) as a function of the diameter of the sample tube, for an annular probe of diameter 7 mm. The real part of the error is smaller by at least a factor of 10.

range 0–3 kHz. The deviation from proportionality is negligible for tubes up to 50 mm in diameter, and amounts to only about 5% for a 100-mm tube at 3 kHz. This proportionality to frequency means that, to a good approximation, the impedance error can be thought of as the effect of an inertive impedance jX_{error} in series with the input to the duct being measured. For tube diameters less than about twice that of the inlet annulus, however, the inertance X_{error} is actually negative and is effectively subtracted rather than added.

Exploration of the trend of the error as the diameter mismatch is varied is shown in Fig. 3, where the quantity plotted is X_{error}/ω. For this calculation the contributions of 100 evanescent modes were included in the calculation, since this presents no computational difficulty. If only a much smaller number of modes, say ten, is included, then the curve, while following the same trend as in Fig. 3, exhibits oscillations as a function of tube diameter. The error is almost exactly proportional to frequency over the measurement range 0–3 kHz used, so that the curve in Fig. 3 applies at all frequencies in this range. For large tube diameters, but still below the higher-mode propagation frequency, $X_{\text{error}}/\omega \rightarrow 40 \, \text{Pa s}^2 \text{m}^{-3}$, which is about equal to the impedance of a short stub tube matching the inlet annulus in diameter and with a length about equal to 0.4 times its radius. This is, as might be expected, comparable to the magnitude of the imaginary part of the radiation impedance for a vibrating circular disc of this size set in an infinite plane baffle. Interestingly, the mismatch error passes cleanly through zero for a tube diameter of about 15 mm, about twice the probe inlet diameter, and then increases in magnitude again, but with a negative sign, for narrower tubes. The reason for this change is that, as the diameter is increased, zeros of the lower-order Bessel functions $J_0(\alpha_n r/R)$ pass successively across the inlet annulus so that their excitation, as seen from the microphone position at $r=0$, shifts from negative to positive. The mode with $n=1$ is particularly important in this connection.

What is important, however, is not the absolute value of the error but rather its magnitude relative to the impedance quantity being measured. A useful measure of this can be
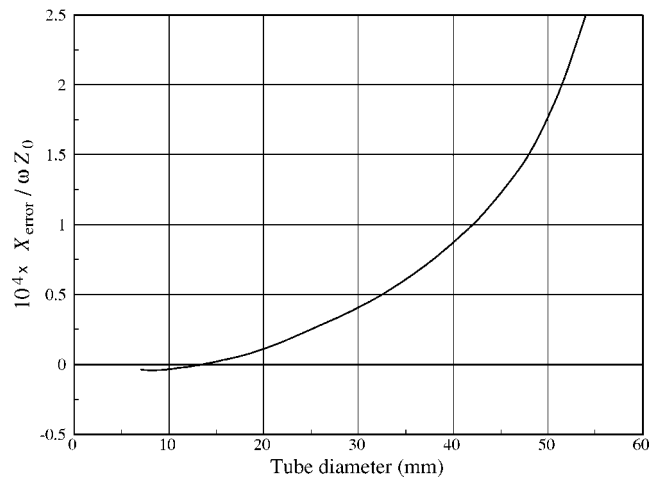

FIG. 4. Calculated frequency-weighted relative error $X_{\text{error}}/\omega Z_0$ in the imaginary part of the impedance (in units of seconds) as a function of the diameter of the sample tube for the case of an annular probe diameter of 7 mm. The real part of the error is smaller by at least a factor of 10. Since typically $\omega \sim 10^4 \, \text{s}^{-1}$, the error is comparable to the value of Z_0 over most of the diameter range shown for frequencies below about 3 kHz. As discussed in the text, this curve is not universal but must be further scaled by a factor $\omega a/c$.

reached by dividing the frequency-weighted absolute error X_{error}/ω of Fig. 3 by the characteristic impedance $Z_0(R) = \rho c/\pi R^2$ of the tube being measured. This frequency-weighted relative error $X_{\text{error}}/\omega Z_0(R)$ is shown in Fig. 4 as a function of tube radius R. The mismatch range covered is the same as in Fig. 3. From Fig. 4 it is clear that the relative error is small for ducts up to about three times the probe annulus diameter, while for ducts of larger diameter the relative error increases about as the square of the diameter mismatch to the probe. For mismatch ratios larger than about 7 the error is so large that accuracy is severely compromised even after correction. Note incidentally that, from the form of (17), the curve in Fig. 4 is not universal, but must be scaled by a further factor $\omega a/c$.

IV. ALTERNATIVE PROBE GEOMETRIES

The first geometrical variant that should be considered is the assumption made in the previous analysis that the width of the inlet annulus is essentially zero and that the diameter of the microphone is also zero. The first of these assumptions is generally a good approximation, since the diameter of the annulus is typically of order 10 mm while its width is typically only about 0.1 mm. The second assumption is, however, far from being realized in practice, since the microphone diameter is typically about 2 mm, which is an appreciable fraction of the annulus diameter. The effect of this is that, if the probe is connected to a duct of matching diameter for calibration, the contributions of modes for which the first radial zero lies within the radius of the microphone will be very greatly reduced, since positive and negative contributions will be averaged over the microphone surface. Since the sharp minimum in X_{error} shown in Fig. 3 for a microphone of zero diameter in a tube closely matching the probe diameter is largely due to these high-order modes, the impedance correction implied for this situation is actually

exaggerated, typically by as much as a factor of 2. A detailed analysis will not be given here, but essentially it involves integration over the area of the microphone, though to a reasonable approximation a similar result is obtained simply by ignoring the contributions of the higher modes. This matter will be revisited in Sec. VII. As shown in Fig. 4, however, the relative correction for tubes with diameter mismatch less than about a factor of 2 is actually very small, so that the problem is not serious until large mismatches are involved, and a solution for this practical problem is presented in that section.

As an alternative, consider the geometry illustrated in Fig. 1(b), in which the measurement microphone is now offset from the axis defined by the inlet annulus. The analysis of this case proceeds just as before except that allowance must be made for the offset of the microphone. Let us take this offset to be $r = b$ for generality. Equation (13) then becomes

$$Z_{\text{meas}} = \frac{p}{U}\bigg|_{x=0, r=b} = \frac{1}{U}\left(\sum_{n=0}^{\infty} A_n J_0\left(\frac{\alpha_n b}{R}\right) + B\right), \qquad (19)$$

and (15) becomes

$$Z_{\text{meas}} = Z_{\text{true}} + \sum_{n=1}^{\infty} \frac{\omega\rho}{2\pi k_n M_n} J_0\left(\frac{\alpha_n a}{R}\right) J_0\left(\frac{\alpha_n b}{R}\right). \qquad (20)$$

For the particular case in which $b = a$ and the microphone is set at a point upon the inlet annulus, the final term of (20) contains the factor $J_0^2(\alpha_n a/R)$, which is always positive, so that the error term is itself always positive, rather than becoming negative for values of R less than about $3a$, as calculated for the central microphone with $b = 0$. Other geometries are similarly easily calculated.

Another probe geometry of interest is that in which the microphone is set forward of the plane of the injection annulus by a small amount δ. Clearly, if $\delta > R$, then most of the evanescent waves will have decayed to negligible amplitude at the microphone position and will not influence the measurement. The impedance that is measured, however, will then not be the true impedance at the inlet port but rather that at the displaced position. While calculation of the necessary correction is possible, its value depends upon the impedance being measured, so that this is not a realistic approach for a general-purpose impedance probe if the diameter mismatch is large.

In real probe geometries, of course, the microphone diameter is not zero, and this must be taken into account by integrating the sensed pressure signal across the microphone area. In most cases this will slightly reduce the value of the necessary correction, since the higher evanescent modes with wavelength smaller than the microphone diameter will have a much reduced effect.

V. RESISTIVE CORRECTION

There is, however, one significant thing that has been omitted from the analysis detailed so far, and that is the possibility of a resistive component to the error contributed by the evanescent modes. Because all the acoustic motion associated with these modes is localized within a distance of about R/α_n of the entry plane, and because there is a signifi-

cant component of acoustic motion that is tangential to this plane, certain losses are to be expected. The magnitude of these losses should be about inversely proportional to the boundary layer thickness, and should thus vary as $\omega^{1/2}$.

In a formal sense, these effects lead to the arguments of the Bessel functions in Eq. (2) being complex rather than real, but this formal analysis has not been carried out because there will inevitably be a significant correction factor that depends upon the roughness of the surface of the inlet plane, including the microphone, and the possible presence of sharp edges. Since the correction due to this effect is small compared to the reactive component of the error already considered, it will therefore be left as a small adjustable parameter.

VI. APPLICATION TO A CALIBRATED PROBE

Researchers at this laboratory have developed an acoustic impedance probe of the general type shown in Fig. 1, though with several geometrical variations, and have devised a calibration procedure that makes its results very accurate for inlet tubes of specified diameter.[9,10] In the calibration procedure, the probe is connected to an effectively semi-infinite pipe (actually 40–200 m in length, depending upon the pipe diameter, so as to produce an attenuation of about 80 dB in the reflected wave for the frequency range of interest) closely matching it in diameter. The flow annulus is fed with a sound pressure signal made up of a very large number of independently adjustable components with a frequency separation of typically about 2.7 Hz. The response of the computer-controlled pressure measurement system is then adjusted in phase and amplitude so that both these measured quantities are constant over the frequency range of interest. (There are actually some experimental subtleties about this that need not be considered here.) The acoustic volume flow is then taken to be this pressure divided by the characteristic impedance $\rho c/S$ of the effectively semi-infinite calibration tube, and these settings are then used in subsequent measurements. This procedure cancels out all evanescent mode effects as well as all irregularities in phase or amplitude of the injected flow or the microphone response for this tube diameter. Measurements on objects with an input duct closely matching the calibration tube in diameter are therefore highly accurate.

It is clearly impractical to have such very long calibration tubes of all diameters available, so that there are restrictions on the applicability of this calibration technique. If the probe is calibrated on a tube closely matching the inlet annulus in diameter, as is usual, then the calibration procedure effectively adds an inertive impedance in order to cancel out the negative imaginary part of the impedance error shown in Fig. 3. If this calibrated probe is then used to make measurements on an object with a much larger inlet pipe diameter, an additional positive error will be introduced into the imaginary part of the measured impedance. The effect of the correction will then be effectively added to the error. This complication can, however, be largely removed by programming the measurement system to subtract off a positive imaginary impedance of magnitude appropriate to correct for the difference between the errors for the measurement tube and the calibration tube.

J. Acoust. Soc. Am., Vol. 117, No. 5, May 2005

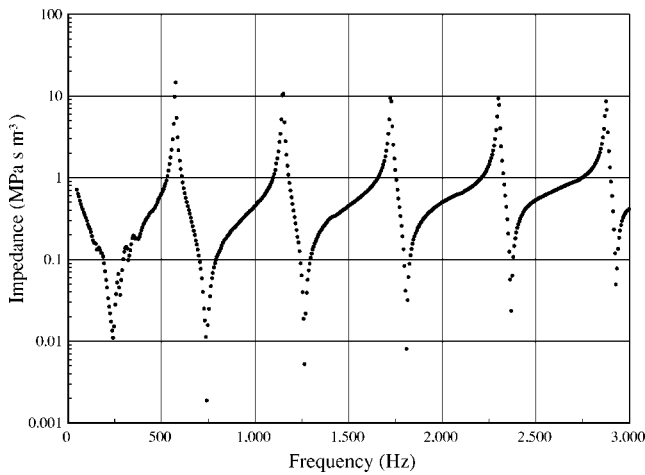Fletcher *et al.*: Acoustic impedance measurements   2893

FIG. 5. Measured magnitude, without correction, of the impedance of a stopped tube 300 mm long and 48 mm in diameter, as measured using the impedance probe described, with an inlet annulus diameter of 6.5 mm, calibrated on a tube of diameter 7.8 mm. Individual measurement points are shown.

Fortunately, the laboratory for which the impedance probe was designed studies the acoustics of musical wind instruments and of the vocal tract, so that only a narrow range of tube diameters is involved, and a set of calibration pipes with appropriate diameters (from 3 to 26 mm) and lengths between 42 and 197 m has been installed without undue expense.

VII. EXPERIMENTAL VERIFICATION

As a check with experiment, an impedance probe with the geometry shown in Fig. 1(a), with inlet annulus mean diameter 6.5 mm and width 0.1 mm and with a centrally located microphone of diameter 1.9 mm was calibrated on a long tube of diameter 7.8 mm, using the procedure previously described.[9,10] When this probe was used to measure the magnitude of the impedance of a rigidly stopped brass pipe of diameter 48 mm and length 300 mm, the results were as shown in Fig. 5. The magnitude and phase of the impedance were measured at each point, and the measurement points are shown in the figure. The characteristic impedance $\rho c/S$ for this pipe is about 0.23 MPa s m^{-3}, and the minima should be located centrally between successive maxima, so that it is clear that the raw measurements are greatly in error. The resemblance of the graph to that calculated in Fig. 2 is clear. The poor signal-to-noise ratio apparent below about 300 Hz is the result of the peculiar measurement configuration chosen for this test. Normally a much smaller mismatch in diameter would have been chosen for the measurement, and the concentric geometry used here for the test transmits a much larger vibration signal to the microphone than does the off-axis geometry normally used in this particular probe.[9,10]

To correct the measurements, the errors for both the calibration tube and the measurement tube must be considered. To further refine the correction, use can be made of the scaling law (17) since the actual diameter of the inlet annulus was 6.5 mm rather than the 7 mm used to calculate Fig. 3. This involves small changes to both the ratio R/a and the factor $\omega a/c$, but these will be neglected here. It is first noted
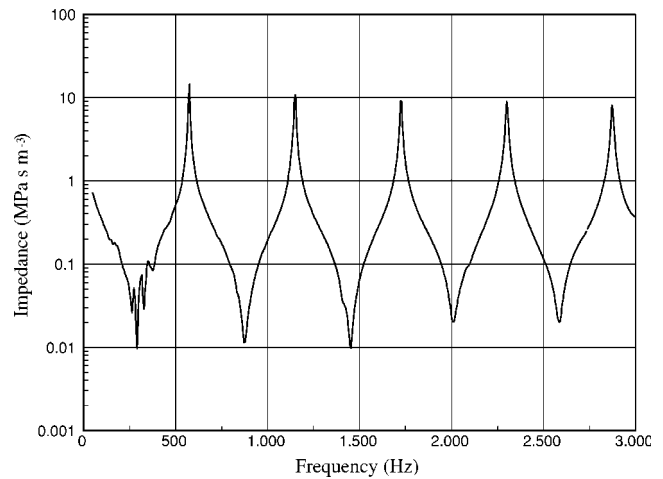

FIG. 6. Measured magnitude of the impedance of the stopped tube of Fig. 5 when corrected by subtracting a series impedance of $(200\omega^{1/2} + 41j\omega)$ Pa s m^{-3}.

from Fig. 3 that the correction for the calibration pipe is negative, since its diameter is close to that of the inlet annulus. Its value from Fig. 3, which assumed a microphone of zero diameter, is about $-30j\omega$ Pa s m^{-3}. As discussed briefly in Sec. IV, however, the fact that the microphone diameter is actually nearly 2 mm eliminates most of the contribution of modes with $n>10$ so that the real correction is only about half this much, or about $-15j\omega$ Pa s m^{-3}. The large pipe, then, is about seven times the diameter of the annulus, so that the equivalent value of diameter in Fig. 3 is about 45 mm, for which the correction is positive and equal to about $30j\omega$ Pa s m^{-3}. Since the probe was calibrated so as to give zero error on the narrow calibration pipe, it is the difference between the two errors, and thus about $45j\omega$ Pa s m^{-3}, that must be used in correcting the measurement error on the wide pipe. A certain amount of latitude is allowable when making this correction, however, since the effect of nonzero microphone diameter and the slight difference in annulus diameter were only approximately allowed for. A value of $41j\omega$ Pa s m^{-3}, which is quite close to the estimate of $45j\omega$ Pa s m^{-3}, gives a well-corrected result for the frequencies of the impedance minima, as shown in Fig. 6.

If only the imaginary contribution to the correction is considered, however, then the impedance minima are rather shallow, and it is necessary to include the resistive contribution as well. As discussed in Sec. V, it is difficult to estimate the magnitude of this correction, so that trial-and-error is the best approach. In the present case it turns out to be necessary to subtract a resistive correction of $200\omega^{1/2}$ Pa s m^{-3} in order to achieve the appropriate symmetry between impedance maxima and minima, as shown in Fig. 6. Over the frequency range considered, this resistive correction is less than 10% of the inductive correction and affects only the sharpness of the impedance minima.

The correction for the case illustrated in Figs. 5 and 6 is an extreme one, and would not ordinarily be used because the noise in the measurement then becomes noticeable. It would, however, be adequate if an approximate measurement were required and only a narrow probe were available. Rather than relying upon the calculations outlined in the

Fletcher *et al.*: Acoustic impedance measurements

present paper, however, the best method for determining and applying the necessary correction is probably as follows:

(1) Calibrate the probe in the usual way on a semi-infinite pipe.
(2) Use this calibrated probe to measure the impedance of a stopped pipe with diameter equal to that of the object to be measured and of such a length that it shows several impedance maxima and minima in the proposed measurement range. Record the results. (The maxima will be correct but the minima will be displaced.)
(3) Write a computer program to subtract from the measured impedance a correction $A\omega^{1/2}+jB\omega$, with A and B as real constants and $A>0$, and display the result. Vary the magnitude of B until the minima are as nearly as possible half-way between the maxima; then vary the magnitude of A until the envelope of the minima matches that of the maxima. If a very wide frequency range and/or a very large geometrical mismatch is involved, then the correction can be of the form $A\omega^{1/2}+jB\omega(1+C\omega)$ with $|C\omega|\ll1$ at the upper frequency limit.
(4) Record this correction and use it to correct all measurements made on devices coupled to the impedance probe through tubes of that diameter.

VIII. CONCLUSIONS

A method has been described that allows calculation of the errors introduced in acoustic impedance measurements when there is a geometrical mismatch, particularly a size mismatch, between the impedance probe and the inlet tube to the device being measured. While this calculation has been carried out for the simplest and most symmetrical geometrical mismatch situations, the methods can clearly be extended to apply to more complex cases, including those in which the microphone is offset both from the axis of the probe and from its inlet plane, or in which the geometry has a symmetry other than circular. Comparison with experiment shows that even quite extreme mismatches in diameter can be corrected for in this way.

This correction approach is not advocated when precise measurements are required, since the experimental noise in the measurements is then exaggerated when the large series

inductance is subtracted. For such measurements, a probe of comparable diameter should be used, and this should be calibrated using an effectively infinite pipe closely matching in diameter the input diameter of the object under test.

While this analysis has been performed for the case of an acoustic probe using a high-impedance inlet duct, a very similar result would be obtained for the case of a probe in the form of a standard standing-wave impedance tube. There is, however, an additional complication in this case since the input flow cannot be assumed to be uniform across the whole inlet tube—the influence of evanescent modes within this inlet tube itself must therefore be taken into account.

An ideal design of impedance probe that would overcome these problems would be one in which, instead of using a localized acoustic flow inlet in the form of a very narrow annulus or other convenient geometry, the flow was injected instead through a high-impedance porous-solid plug extending across the whole area of the inlet to the object being measured. Even in this case, however, a calibration procedure using an effectively infinite pipe is desirable in order to compensate for any possible frequency dependence of the flow impedance or of the associated electronic equipment.

[1] L. L. Beranek, *Acoustic Measurements*, revised edition (Acoustical Society of America, New York, 1988), pp. 294–353.
[2] A. H. Benade and M. I. Ibisi, "Survey of impedance methods and a new piezo-disk-driven impedance head for air columns," J. Acoust. Soc. Am. **81**, 1152–1167 (1987).
[3] N. H. Fletcher and T. D. Rossing, *The Physics of Musical Instruments*, 2nd ed. (Springer-Verlag, New York, 1998), pp. 222–223.
[4] J. Backus, "Input impedance curves for the reed woodwind instruments," J. Acoust. Soc. Am. **56**, 1266–1279 (1974).
[5] M. Abramowitz and I. A. Stegun, *Handbook of Mathematical Functions* (National Bureau of Standards, Washington, DC, 1964), p. 411.
[6] A. H. Benade, "On the propagation of sound waves in a cylindrical conduit," J. Acoust. Soc. Am. **44**, 616–623 (1968).
[7] M. Abramowitz and I. A. Stegun, *Handbook of Mathematical Functions* (National Bureau of Standards, Washington, DC, 1964), formula 11.3.34.
[8] W. H. Press, B. P. Flannery, S. A. Teukolsky, and W. T. Vetterling, *Numerical Recipes* (Cambridge U.P., Cambridge, 1986), Sec. 6.4.
[9] J. Wolfe, J. Smith, G. Brielbeck, and F. Stocker, "A system for real time measurement of acoustic transfer functions," Acoust. Aust. **23**, 19–20 (1995).
[10] J. Wolfe, J. Smith, J. Tann, and N. H. Fletcher, "Acoustic impedance spectra of classical and modern flutes," J. Sound Vib. **243**, 127–144 (2001).